ACS APPLIED MATERIALS & INTERFACES

Research Article

www.acsami.org

Solution-Processed Field-Effect Transistors Based on Dihexylquaterthiophene Films with Performances Exceeding Those of Vacuum-Sublimed Films

Tim Leydecker,[†] Duc Trong Duong,[‡] Alberto Salleo,[‡] Emanuele Orgiu,[*,†] and Paolo Samorì[*,†]

[†]ISIS & icFRC, Université de Strasbourg & CNRS, 8 Allée Gaspard Monge, 67000 Strasbourg, France

[‡]Department of Materials Science and Engineering, Stanford University, Stanford, California 94305, United States

Supporting Information

ABSTRACT: Solution-processable oligothiophenes are model systems for charge transport and fabrication of organic field-effect transistors (OFET). Herein we report a structure vs function relationship study focused on the electrical characteristics of solution-processed dihexylquaterthiophene (DH4T)-based OFET. We show that by combining the tailoring of all interfaces in the bottom-contact bottom-gate transistor, via chemisorption of ad hoc molecules on electrodes and dielectric, with suitable choice of the film preparation conditions (including solvent type, concentration, volume, and deposition method), it is possible to fabricate devices exhibiting field-effect mobilities exceeding those of vacuum-processed DH4T transistors. In particular, the evaporation rate of the solvent, the processing temperature, as well as the concentration of the semiconducting material were found to hold a paramount importance in driving the self-assembly toward the formation of highly ordered and low-dimensional supramolecular architectures, confirming the kinetically governed nature of the self-assembly process. Among the various architectures, hundreds-of-micrometers long and thin DH4T crystallites exhibited enhanced charge transport.

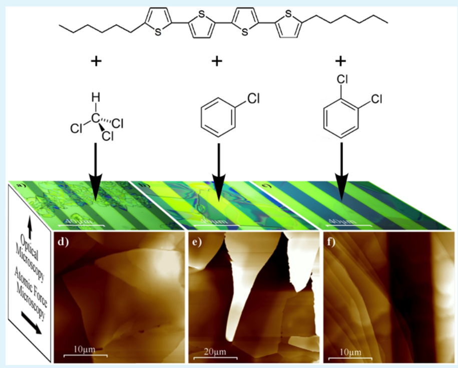

KEYWORDS: *dihexylquaterthiophene, organic field-effect transistors, contact resistance, drop-cast, metal−semiconductor interface, dielectric treatment*

INTRODUCTION

Organic semiconductors have been the focus of extensive research activity during the past decades because they represent key active components for technological applications in optoelectronics, such as large-area electronics, displays, and sensing.[1−7] Numerous are the advantages they hold when compared to their inorganic counterparts, including the tunability of their physical properties via chemical functionalization,[8−10] their low-cost processing[11,12] using mild conditions (low temperature and ambient pressure), and up-scalable approaches even on flexible supports.[13] However, in order to enter the marketplace, most of the solution-processable organic semiconductors still need to reach field-effect mobilities comparable to those of amorphous silicon. These low device mobilities arise from the poor crystallinity of the semiconducting layers due to a typical grain size that is normally much smaller than the channel length of the device.[14] Furthermore, the properties of organic devices are strongly interface-dependent[15,16] given the importance that metal/semiconductor and dielectric/semiconductor play in determining the field-effect transistor's (FET) mobility as well as threshold voltage. Hence, optimal interface engineering is required because it will ultimately affect mobility and threshold voltage. For example, both low interface roughness at the electrode−semiconductor interface and a minimized energy mismatch between electrode and organic material are required in order to attain good charge injection.[17] Controlling the structure of the organic material at the interface can be achieved through chemisorption of self-assembled monolayers (SAM) on both dielectric and electrode surface.[18−22]

Small semiconducting molecules have been the target of a wide research endeavor in the last decades and have proven to exhibit interesting electrical performances, partly due to their more pronounced tendency to form crystalline domains when compared to their polymeric counterparts.[23−29] Among all organic small molecules, pentacene, rubrene, and 2,7-dioctyl[1]benzothieno[3,2-*b*][1]benzothiophene (C_8-BTBT) have so far exhibited the largest carrier mobilities, up to μ = 43 $cm^2/(V\ s)$, in off-center spin-coated C_8-BTBT film.[30−32] In addition to the above-mentioned families of small molecules, a substantial activity has been devoted over 2 decades to oligothiophenes as promising candidates for charge transport.[33−36] Initially they were deposited by means of thermal evaporation,[37,38] until substituted moieties were synthesized, making it possible to process them from solution.[39,40] In particular, hexamethyl-substituted oligothiophene-based devi-

Received: September 12, 2014
Accepted: November 7, 2014
Published: November 7, 2014

 © 2014 American Chemical Society

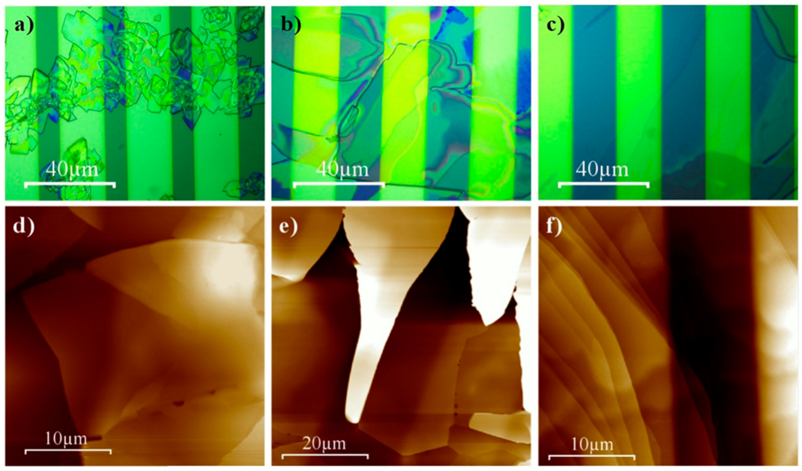

Figure 1. Top panel: Optical microscope images of DH4T films produced by drop-casting solutions in (a) $CHCl_3$, (b) CB, and (c) DCB. Bottom panel: Tapping mode AFM topography images of DH4T films produced by drop-casting solutions in (d) $CHCl_3$, (e) CB, and (f) DCB. *Z*-scales: (d) 2 μm, (e) 500 nm, and (f) 120 nm.

ces, such as those using dihexylquaterthiophene (DH4T), are easily accessible model systems that have proven to display a high resistance to the environment, due to their dense packing and hexyl chains working as a passivation layer[41−43] in addition to their charge transport performance in transistors.[44] Indeed, a previous work reported mobilities up to 0.23 $cm^2/(V\ s)$ for thermally evaporated DH4T.[45] However, these performances have only been achieved for a particular channel's width-to-length (W/L) ratio of 1.5 and by using vacuum deposition as a preparation technique. Clearly such a low W/L is not optimal for low-power devices given that very high operating voltages must be applied in order to achieve the same output currents one can measure in devices featuring high W/L ratio. On the other hand, for vacuum-deposited films, the highest observed mobility amounted to 0.09 $cm^2/(V\ s)$, even when a higher width-to-length ratio was used.[46] As far as solution-processed films are concerned, the highest reported mobilty values amounted to $\mu = 0.043$ $cm^2/(V\ s)$ for ink-jet-printed devices[47] and $\mu = 0.012$ $cm^2/(V\ s)$ for spin-coated films,[48] indicating that there is much room for improvement on the processing side. Further, the statistical deviation of the average mobilities as well as the number of measured samples are seldom reported, thereby lessening the reliability of the estimated materials properties. The I_{on}/I_{off} ratio reported in the literature for this material usually ranges between 10^5 and 10^7,[45−47] providing evidence for the good switching ability of the devices. Morphology and crystallographic parameters of DH4T films have been more recently investigated by Thierry and co-workers, who showed how DH4T can self-assemble into a highly ordered crystalline structure.[49] In their study, the crystalline order within domains produced by vacuum sublimation was similar to that found in crystalline domains grown from solution. High mobility solution-processed devices can be therefore produced if the kinetically governed process of film growth is controlled to achieve large crystalline domains,[50] eliminating or reducing the effect of grain boundaries, which are detrimental for the charge transport.[51−53]

In this work, by attaining control over the kinetics of the self-assembly process via the optimization of the solvent evaporation rate combined with a careful choice of the source/drain and gate dielectric surface functionalization, we have fabricated via drop-casting DH4T-based FETs exhibiting charge carrier mobility as high as 0.1 $cm^2/(V\ s)$, therefore exceeding the reported values measured in thin-film transistors with a vacuum-sublimed active layer.

EXPERIMENTAL SECTION

The tested molecule was purchased from Polyera under the name ActivInk P0400 and used as received, without further purification. Solvents were purchased from Sigma-Aldrich and used as provided. Bottom-contact bottom-gate configuration transistors purchased from Fraunhofer Institute were used. They consist of n^{++}-Si substrates with 230 nm of thermally grown SiO_2 as the gate dielectric (15 nF capacitance) and prepatterned pairs of gold electrodes with interdigitated geometry as the source and drain. All samples were prepared and measured in a N_2-filled glovebox to avoid oxidative doping of the materials and ensure reproducibility of the experiments. Solution preparation, hexamethyldisilazane (HMDS) treatment, and electrode functionalization were performed under nitrogen atmosphere. The electrodes were functionalized by immersion a 4 mM solution of 1-decanethiol (C_{10}) in ethanol for 12 h. C_{10} has been selected to increase the wetting abilities of the wafer. Substrates were thoroughly rinsed by squirting with 100 μL of absolute ethanol five times. HMDS and octadecyltrichlorosilane (OTS) were both purchased from Sigma-Aldrich. HMDS was spin-coated at 1500 rpm on the substrate and annealed for 1 h at 100 °C. The 5 mg/mL solution was prepared by dissolving 5 mg of DH4T in 1 mL of 1,2-dichlorobenzene. The solution was afterward stirred and heated at 100 °C for 1 h, and 70 μL of the cold solution was drop-cast on the substrate. Drop-casting was chosen as the deposition technique since, compared to spin-coating, it is more similar to the ink-jet-printing process used in real device fabrication. After drop-casting, films were dried up at room temperature for 4 days under a Petri dish to slow the evaporation in order to achieve higher crystallinity.

The properties of organic field-effect transistors (OFET) were evaluated under positive or negative gate bias to explore the majority charge carrier type and device performance. Experimental data were analyzed using standard field-effect transistor equations (for p-type semiconductors):

$$I_{DS} = -\frac{W}{2L}\mu C_0(V_{GS} - V_{Th})^2$$

where I_{DS} is the source-drain current, V_{GS} is the gate voltage, C_0 is the capacitance per unit area of the dielectric layer, V_{Th} is the threshold voltage, and μ is the field-effect mobility in the saturation region. The mobilities were determined in the saturation regime, i.e., at $V_{DS} = -60$ V from the slope of plots of $I_{GS}^{1/2}$ versus V_{GS}. In all the characterized

Table 1. Detailed Correlation between DH4T Processing Conditions, Solvent Employed, and Electrical Performances[a]

solvent	SAM	volume (μL) of DH4T cast, concn (mg/mL)	evaporation rate (butyl acetate = 1)	av[g] mobility [$cm^2/(V\ s)$]	I_{ON}/I_{OFF}	av[g] V_{Th} (V)
$CHCl_3$	HMDS	100, 1	11.6	6.85×10^{-5}	10^1–10^4	−12
CB[b]	HMDS	100, 1	0.2[d]	1.09×10^{-3}	10^1–10^4	−7
DCB[c]	HMDS	100, 1	0.2[d]	6.63×10^{-3}	10^4–10^6	−8
DCB[c]	HMDS	70, 5	0.2[d]	8.80×10^{-3}	10^4–10^5	−37
DCB[c]	HMDS	100, 3.5	0.2[d]	1.11×10^{-2}	10^4–10^5	−36
DCB[c]	HMDS	70, 10	0.2[d]	4.34×10^{-4}	10^1–10^3	−14
DCB[b]	HMDS	70, 2	0.02[f]	7.70×10^{-4}	10^2–10^3	−45
DCB[c]	HMDS	70, 5	0.02[f]	3.33×10^{-3}	10^4–10^5	−39
DCB[c]	HMDS	100, 3.5	0.02[f]	2.00×10^{-3}	10^3–10^5	−43
DCB[c]	HMDS	70, 5	0.1[e]	2.58×10^{-2}	10^4–10^5	−39
DCB[c]	OTS	70, 5	0.1[e]	6.14×10^{-2}	10^7	−10

[a]All films were drop-cast on HMDS-treated silicon oxide and untreated gold electrodes. [b]Chlorobenzene. [c]Dichlorobenzene. [d]Solvent left to evaporate at a normal rate (evaporation taking between 12 and 18 h). [e]Solvent left to evaporate at a slow rate (evaporation taking between 1 and 2 days). [f]Solvent left to evaporate at a very slow rate (evaporation taking between 5 and 7 days). [g]Average over at least 16 devices.

sets, the voltage range was kept constant for both I_{DS}–V_{DS} and I_{DS}–V_{GS} to ensure full comparison among different samples.

In order to evaluate the contact resistance (R_C), the conductivity as a function of the channel length has been measured for >110 devices. By subtracting the parasitic contribution of the contact resistance from the total measured resistance ($R_{measured} = R_{total} = R_{channel} + R_c$), the field-effect mobility values could be adjusted.

For each device (2.5, 5, 10, and 20 μm channels) the inverse of the transconductance (g_m), which takes into account the whole resistive contribution coming from both material and contacts, has been extracted from the I_{DS}–V_{GS} graphs in the linear regime.

$$R_{total} = (g_m)^{-1} = \left(\frac{\partial I_{DS}}{\partial V_{GS}}\right)^{-1}$$

R_{total} values have been plotted as a function of the channel length for four samples at both $V_{DS} = -20$ V and $V_{DS} = -25$ V. The resistance calculated at channel length (L) = 0 μm is the contact resistance contribution to the total resistance.

An ambient photoelectron spectrometer (AC-2, by RKI Instruments) working at ambient conditions was employed to determine the ionization energy (IE) of the DH4T films and the work function of the different SAM-functionalized gold electrodes. The morphology of the large crystallites has been mapped by performing topographical AFM imaging in tapping mode in air environment using a Veeco Dimension 3100 operating on a Nanoscope IV control unit.

■ RESULTS AND DISCUSSION

Initially this prototypical molecule was tested in three different chlorinated solvents, namely, chloroform ($CHCl_3$), 1,2-dichlorobenzene (DCB), and chlorobenzene (CB). The choice of the solvent was found to be crucial for the device performance. In particular, multiscale morphological characterization, from the hundreds-of-micrometers down to submicrometer scale, was carried out both by optical (OM) and atomic force (AFM) microscopy, therefore supporting the electrical and structural characterization presented later in the paper.

Figure 1 compares the morphologies of DH4T films prepared by drop-casting a 100 μL drop on a SiO_2/Si-n^{++} substrate from 1 mg/mL concentrated solution in $CHCl_3$, CB, and DCB. The surface of the DH4T films deposited from chloroform solution (Figure 1a,d) consists of small crystals, often not interconnected, whereas the films obtained using chlorobenzene or dichlorobenzene as a solvent (Figure 1b,e and c,f) display larger and more uniform crystalline domains in OM images. The film uniformity without the presence of defects over a larger scale for chloro- and dichlorobenzene films does significantly decrease the occurrence of grain boundaries. Conversely, films deposited from $CHCl_3$ displayed very high surface roughness on the mesoscale [root-mean square roughness (R_{rms}) of 165 nm; see Figure 1d and Table S7 (Supporting Information, SI)], while films prepared from CB showed a decreased roughness (R_{rms} = 22 nm). Films prepared from DCB solutions exhibited an even smaller roughness (with R_{rms} = 7 nm).

Optical microscope images confirm that when the optimized procedure (described below) is used, the crystallites processed from DCB solvent are large enough to easily bridge the source-drain electrodes for channel lengths up to 20 μm (Figure S1, SI). For longer channel lengths, such as 60 μm, the crystallites are only slightly larger than the channel, leading to the presence of more grain boundaries within the channel. The flat crystalline samples prepared from CB exhibit a greater roughness, and more grain boundaries are present while those from chloroform tend to form extremely rough aggregates (Figure 1).

When employed as the active layer in a bottom-contact bottom-gate FET with Au source and drain electrodes, drop-cast films from solution in $CHCl_3$ exhibited 2 orders of magnitude lower mobility and I_{on}/I_{off} when compared to those obtained by using DCB as a solvent. A careful concentration-dependent study was carried out in order to find out the concentration giving the highest mobility (Table 1). The best mobility was recorded when a 5 mg/mL solution was drop-cast from DCB [0.038 $cm^2/(V\ s)$]. Details on electrical performances measured in spin-coated films formed from different solvents are provided in the SI. Furthermore, the evaporation rate of the solvent was found to be a critical parameter when producing DH4T-based OFETs by solution processing. A 3-fold improvement of the charge carrier mobility in drop-cast films was achieved when the evaporation rate was slightly reduced (by a factor of 2) by means of a top cover with a controlled aperture surface. However, when the evaporation rate was more extensively reduced (tightly sealed cover), a drop in mobility appeared up to a factor of 10. As can be seen on the OM images provided in the SI (Figure S3), the evaporation rate of 0.1 produced the film with the least amount of defects. This is due to the solvent-vapor annealing[54] caused by the tightly sealed cover. All of the results are summarized in Tables 1 and S11 (SI).

The procedure that exhibited the best mobility, i.e. 70 μL of DH4T at 5 mg/mL drop-cast from DCB, evaporation rate of

0.1, will be referred to as the "*optimized procedure*". It has been successfully reproduced on >110 devices using HMDS as a surface treatment. Noteworthy, in spite of the fact that drop-casting is a deposition technique which is supposed to lead to uneven device-to-device performances due to thickness variation in the $x-y$ plane, the presence of large, flat crystals spanning over hundreds of micrometers allowed for the fabrication of devices whose electrical parameters featured mobilities with standard deviations that were absolutely comparable to those achieved in spin-coated films (Table S11, SI). In very few instances (less than 3% of the cases), the presence of nonfunctioning devices could be ascribed to the insufficient coverage of the device upon deposition of the material. As highlighted by AFM and OM, the major differences in mobility between the above-mentioned cases would all stem from the occurrence of grain boundaries in the crystalline films, which exhibited a highly crystalline nature as confirmed by grazing incidence X-ray diffraction (GIXD) analysis (see SI).

When the optimized procedure is used (Figure 2), the crystallites readily bridge the source and drain electrodes.

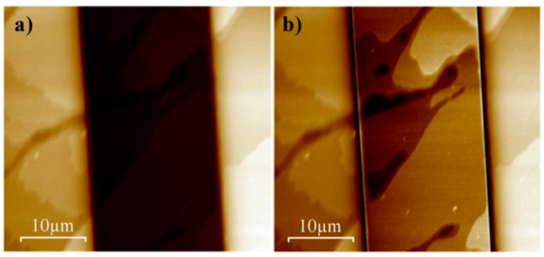

Figure 2. Tapping mode topography AFM images of DH4T crystallites in a 20 μm channel. (a) Unmodified image and (b) linear height flattening introduced in the image to show differences between channel and electrodes. *Z*-scales = 70 nm.

Furthermore, the morphology of the crystallites, bridging and following the profile of the electrodes, seems to suggest the absence of nucleation sites in the interelectrodic region. This indicates that the formation of the crystallites does commence in the solvent and only later these structures "land" on the electrodes and expand via self-assembly.

In addition to the effects of the solvent and its evaporation rate on the electrical performances, a thorough physicochemical analysis of the metal/semiconductor interface was performed. In particular, the gold electrodes were functionalized with either 1-decanethiol [$CH_3(CH_2)_9$-SH] or 1*H*,1*H*,2*H*,2*H*-perfluorodecanethiol [$CF_3(CF_2)_7CH_2CH_2$−SH], forming chemisorbed self-assembled monolayers (SAM). By means of an ambient photoelectron spectroscopy, we measured an ionization energy of 4.96 ± 0.02 eV for DH4T films, while the work function of uncoated gold, 1-decanethiol-functionalized gold, and perfluorodecanethiol-functionalized gold resulted 4.80 ± 0.20, 4.32 ± 0.02, and 5.43 ± 0.02 eV, respectively. Interestingly, the best energy match for injecting holes in the HOMO of DH4T should be attained when perfluorodecanethiol SAMs are employed, followed by uncoated gold and 1-decanethiol-functionalized electrodes. However, both mobility and currents were found to be higher when functionalized electrodes were utilized, revealing that the affinity of the semiconductor for the surface and the physical interface metal/electrode play key roles. In fact, the surface energy of SAM-functionalized electrodes is lower than in uncoated gold, as revealed through contact angle measurements using DCB as liquid. Among the three different cases, the best performing devices were ultimately those bearing SAM-functionalized source and drain electrodes, owing to a lower surface energy and higher surface affinity of the DH4T molecules. To verify the latter statement, we performed contact angle measurements by using solutions of DH4T in DCB (5 mg/mL) as performed in the case of the corresponding devices. The experiment did not reveal appreciable differences with respect to the former contact angle measurements performed with pure DCB (Figure S18, SI).

In addition, all films encompassed in this study exhibit a high degree of crystallinity, as confirmed by GIXD analysis (Figures S13 and S14, SI); interestingly, the structural order within thin films does not differ significantly between samples fabricated under different preparation conditions. We want to point out here that, in general, OFETs probe only the dielectric−semiconductor interface,[55] while GIXD probes the bulk crystalline structure, which may differ from that of the interfacial layer.[56] Because DH4T tends to crystallize into relatively flat platelets, here we assume that the interface exhibits the same crystalline structure as that of the bulk crystal. Most probably, the difference in mobility does not stem from the crystalline order of the film but rather from the difference in the crystallite size as a result of each specific preparation condition. In other words, a high number of small crystals translates into a high number of grain boundaries, which strongly limit charge transport.

Furthermore, even the devices prepared with the optimized procedure based on the use of HMDS and 1-decanethiols to functionalize the interface of the organic semiconducting material with the dielectrics and electrodes, respectively, show an unfavorable charge injection, as evidenced from the nonlinearity of the output curve at low source-drain voltage (Figure 3). For channel length between 2.5 and 20 μm, a hole mobility of about 0.06 $cm^2/(V\ s)$ is observed on >110 devices, with an average I_{on}/I_{off} ratio of $\sim10^5$ (Table S12, SI). The highest hole mobility observed is 0.08 $cm^2/(V\ s)$ and the highest I_{on}/I_{off} ratio is of $\sim5 \times 10^7$. It is worth pointing out that we did not observe any electron (n-type) transport in any device.

Further, when the size of the channel reaches 60 μm and over, we observed a 4- and 10-fold decrease in mobility and I_{on}/I_{off}, respectively (see SI). The amount of devices with observable semiconducting characteristics is considerably lower as well (37% compared to 97%). The threshold voltage is not affected by the change of the channel length.

The average contact resistance value extracted from $I_{DS}-V_{GS}$ graphs in the linear regime is reported in Table S3 and amounted to ~100 kΩ (103 kΩ) (see the SI). By using the $R_{contact}$ value of 103 kΩ, the mobility was adjusted using $R_{channel}$ instead of R_{total}, provided that $R_{channel} = R_{total} - R_{contact}$. The obtained values are plotted as a function of the channel length. We notice that values of the mobility adjusted for $R_{contact} \sim 100$ kΩ are uniform over all the channel lengths, revealing that mobility is an intrinsic parameter of the material and its value should not depend on a specific channel length. When mobilities are corrected for the contact resistance, we observe an average mobility topping 0.05 $cm^2/(V\ s)$ for the small channels (2.5 and 5 μm) (Figure 4).

Significantly, in contrast to HMDS-functionalized devices prepared with the optimized procedure, output curves do not indicate the presence of a high contact resistance when OTS is used to functionalize the surface of the dielectric silicon oxide

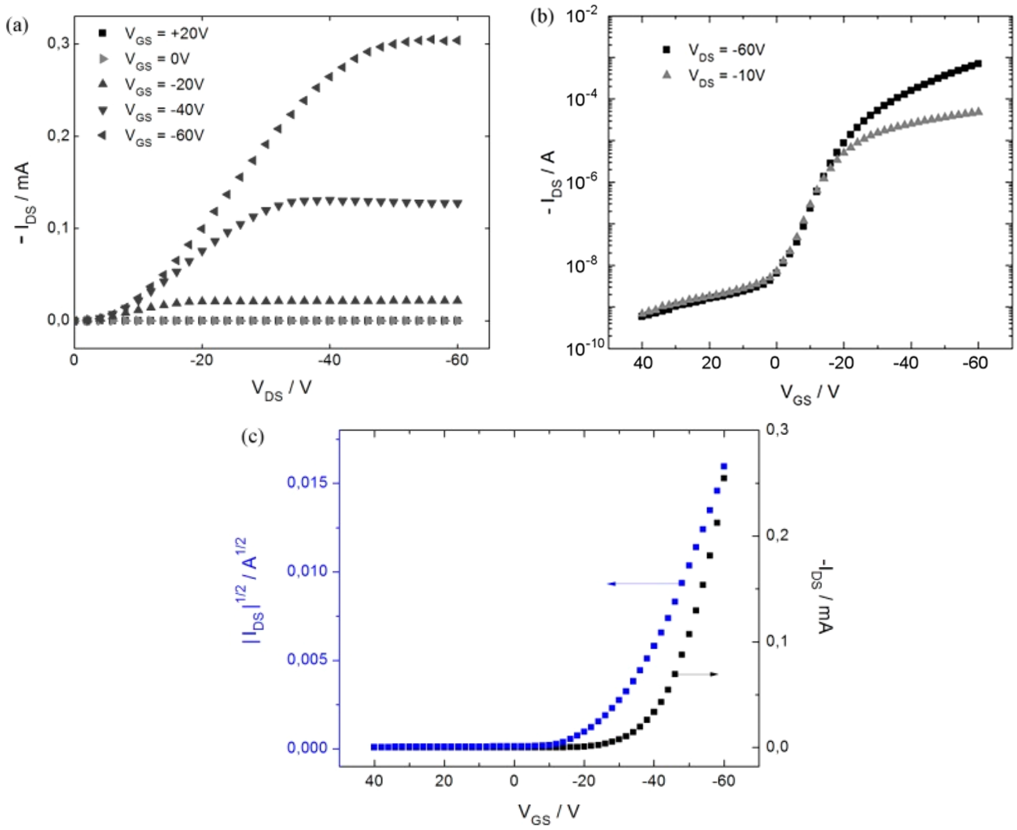

Figure 3. DH4T OFET based on the optimized procedure using HMDS- and 1-decanethiol-treated electrodes. (a) Output characteristics, (b) transfer characteristics of the same device in the linear and saturation region (log scale), and (c) I_{DS} vs V_{GS} and $I_{DS}^{1/2}$ vs V_{GS} in saturation regime (V_{DS} = −60 V, L = 20 μm, W = 10 mm).

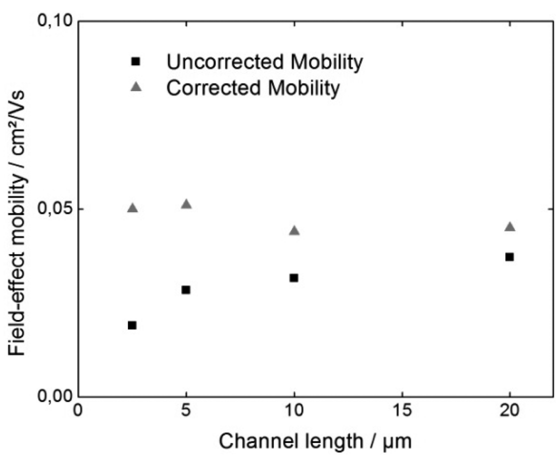

Figure 4. Average field-effect mobility in the saturation regime as a function of the channel length. The devices were prepared according to the optimized procedure on 1-decanethiol-treated gold electrodes.

(Figure 5). The devices exhibit mobilities up to 0.10 $cm^2/(V\ s)$ and I_{on}/I_{off} up to 5 × 10^7. The average threshold voltage was found to be −12 V in the saturation regime, and −9 V in the linear regime, which is 2−3-fold smaller in absolute value when compared to HMDS-treated devices. Figure 5c shows that the transfer curve is bent at high gate voltages. This would indicate that the device is prone to bias stress. Notably, HMDS-treated devices were found to exhibit a more pronounced bias stress when measured at the same $V_{GS} - V_{Th}$ (Figure S11, SI). However, the gate voltage was swept up to −60 V also in OTS-treated FETs for the sake of consistency with the HMDS case. Given that OTS-treated devices showed lower (in absolute value) threshold voltage, the above-mentioned bias stress can be ascribed to the higher $V_{GS} - V_{Th}$ value employed when testing OTS-treated samples.

The reason for these improved electrical performances cannot stem from the chemical difference in the oxide treatment, given that both OTS and HMDS are methyl-terminated. However, the performances on organic transistors are in general improved in terms of threshold voltage and mobility when OTS is utilized.[57] Surprisingly, the dielectric substrate treatment seems to affect the charge injection, as can be observed in the output curves. Several points could be brought up in order to explain this unexpected trend: (i) the DH4T film thickness of OTS-treated devices is thinner than that measured over HMDS ones (tens vs hundreds of nanometers), as confirmed by the AFM and profilometer. (ii) This difference in thickness could lead to higher off current in HMDS-treated devices. In addition, the average off current increase of ca. 2 orders of magnitude can be ascribed to the more favored and unavoidable presence of water molecules on the surface of HMDS- vs OTS-treated silicon oxide, which stems from the larger surface energy of the former. (iii) AFM imaging of films recorded on HMDS-treated substrates showed that they exhibit thinner crystalline planes, lying on top of each other, which are formed during the evaporation of the residual solvent. During the solvent evaporation the crystals will have a certain affinity for the surface. The better interaction of the DH4T crystals for OTS- vs HMDS-treated surface promotes formation of the thickest multilayered crystals in the latter case.

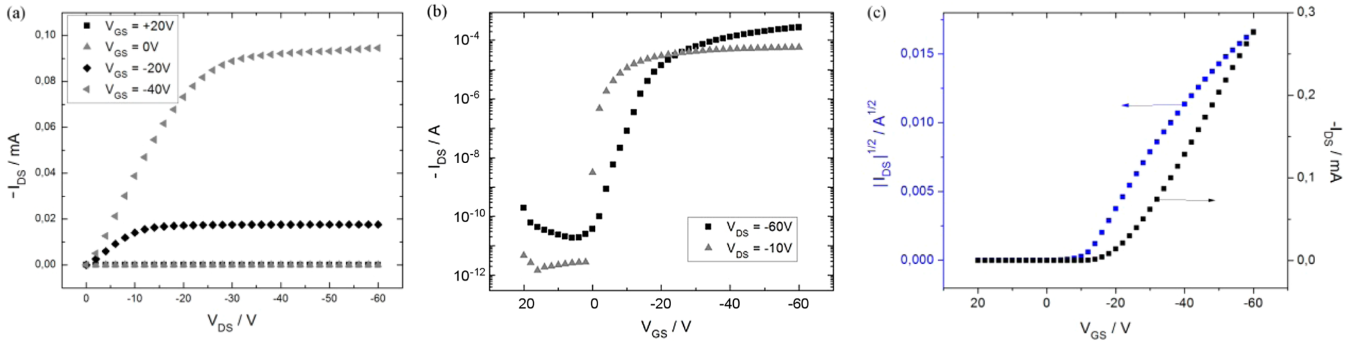

Figure 5. DH4T OFET based on the optimized procedure using OTS- and 1-decanethiol-treated electrodes. (a) Output characteristics, (b) transfer characteristics of the same device in the linear and saturation region, plotted on a logarithmic scale, and (c) I_{DS} vs V_{GS} and $I_{DS}^{1/2}$ vs V_{GS} in saturation regime (V_{DS} = −60 V, W = 10 mm, L = 20 μm).

As a result, the thinner crystalline layers adapt more easily to the prepatterned electrode geometry, therefore improving the semiconductor/electrode interface quality when OTS is used. The presence of more interfacial defects can be further verified by looking at the subthreshold slope and the resulting amount of interfacial traps, which is ca. 10 times lower in OTS-functionalized devices (see Table S6, SI).

■ CONCLUSION

In summary, our comparative study on the structure vs function relationship in solution-processed DH4T-based OFETs revealed that by optimizing the conditions of film formation via judicious choice of processing method, solvent type, interfaces functionalization, and in particular by tuning the rate of evaporation of the solvent, it is possible to drive the molecular self-assembly toward the formation of highly ordered low-dimensional architectures exhibiting enhanced electrical characteristics. Significantly, their use as electroactive components in OFETs led to device performances that are beyond the state-of-the-art for DH4T-base transistors, even when compared to vacuum-processed OFETs made with the same molecule. In particular, p-type mobilities as high as 0.10 $cm^2/(V\ s)$ and I_{on}/I_{off} currents exceeding 10^7 were achieved. Our results unambiguously confirm that the tailoring of interfaces is key. Counterintuitively, the functionalization of the injecting electrodes to render them more hydrophobic, thus optimizing the surface energies via optimal interaction of the alkyl chains of the DH4T for the SAM, is found to be more important than adjusting the energy match with the HOMO of the semiconductor. In addition, we showed how the different silicon oxide treatment can impact directly the assembly of the semiconductor in high boiling point solvents, leading to interfaces with a lower number of interfacial traps, which results in enhanced electrical performances. Our processing method to achieve high-mobility devices is compatible with large-area applications, thus providing a pathway toward organic electronics that satisfies the needed balance between performance and processability.

■ ASSOCIATED CONTENT

Supporting Information

Additional optical microscope images of DH4T, additional electrical characterization of FET devices, grazing incident X-ray diffraction analysis, atomic force microscopy analysis, ambient photoelectron spectrometer measurements, contact angle measurements, and extended tables. This material is available free of charge via the Internet at http://pubs.acs.org.

■ AUTHOR INFORMATION

Corresponding Authors

*E.O. e-mail: orgiu@unistra.fr.
*P.S. e-mail: samori@unistra.fr.

Notes

The authors declare no competing financial interests.

■ ACKNOWLEDGMENTS

This work was financially supported by ERC project SUPRA-FUNCTION (GA-257305), the Agence Nationale de la Recherche through the LabEx project Chemistry of Complex Systems (ANR-10-LABX-0026_CSC), and the International Center for Frontier Research in Chemistry (icFRC). A.S. gratefully acknowledges financial support from the National Science Foundation (DMR 1205752 award). D.T.D. is supported by a Stanford Graduate Fellowship and the National Science Foundation Graduate Research Fellowship.

■ REFERENCES

(1) Sirringhaus, H.; Brown, P. J.; Friend, R. H.; Nielsen, M. M.; Bechgaard, K.; Langeveld-Voss, B. M. W.; Spiering, A. J. H.; Janssen, R. A. J.; Meijer, E. W.; Herwig, P.; de Leeuw, D. M. Two-Dimensional Charge Transport in Self-Organized, High-Mobility Conjugated Polymers. *Nature* **1999**, *401*, 685−688.

(2) Orgiu, E.; Samorì, P. 25th Anniversary Article: Organic Electronics Marries Photochromism: Generation of Multifunctional Interfaces, Materials, and Devices. *Adv. Mater.* **2014**, *26*, 1827−1845.

(3) Tobjörk, D.; Österbacka, R. Paper Electronics. *Adv. Mater.* **2011**, *23*, 1935−1961.

(4) Xu, Y. Y.; Zhang, F.; Feng, X. L. Patterning of Conjugated Polymers for Organic Optoelectronic Devices. *Small* **2011**, *7*, 1338−1360.

(5) Dimitrakopoulos, C. D.; Malenfant, P. R. L. Organic Thin Film Transistors for Large Area Electronics. *Adv. Mater.* **2002**, *14*, 99−117.

(6) Nomoto, K.; Hirai, N.; Yoneya, N.; Kawashima, N.; Noda, M.; Wada, M.; Kasahara, J. A High-Performance Short-Channel Bottom-Contact OTFT and Its Application to AM-TN-LCD. *IEEE Trans. Electron. Devices* **2005**, *52*, 1519−1526.

(7) Torsi, L.; Farinola, G. M.; Marinelli, F.; Tanese, M. C.; Omar, O. H.; Valli, L.; Babudri, F.; Palmisano, F.; Zambonin, P. G.; Naso, F. A Sensitivity-Enhanced Field-Effect Chiral Sensor. *Nat. Mater.* **2008**, *7*, 412−417.

(8) Yoon, M. H.; Facchetti, A.; Marks, T. J. Sigma-Pi Molecular Dielectric Multilayers for Low-Voltage Organic Thin-Film Transistors. *Proc. Natl. Acad. Sci. U. S. A.* **2005**, *102*, 4678−4682.

(9) Nouchi, R.; Kubozono, Y. Anomalous Hysteresis in Organic Field-Effect Transistors with Sam-Modified Electrodes: Structural Switching of SAMs by Electric Field. *Org. Electron.* **2010**, *11*, 1025–1030.
(10) Mei, Y. C.; Loth, M. A.; Payne, M.; Zhang, W. M.; Smith, J.; Day, C. S.; Parkin, S. R.; Heeney, M.; McCulloch, I.; Anthopoulos, T. D.; Anthony, J. E.; Jurchescu, O. D. High Mobility Field-Effect Transistors with Versatile Processing from a Small-Molecule Organic Semiconductor. *Adv. Mater.* **2013**, *25*, 4352–4357.
(11) Forrest, S. R. The Path to Ubiquitous and Low-Cost Organic Electronic Appliances on Plastic. *Nature* **2004**, *428*, 911–918.
(12) Yan, H.; Chen, Z.; Zheng, Y.; Newman, C.; Quinn, J. R.; Dötz, F.; Kastler, M.; Facchetti, A. A High-Mobility Electron-Transporting Polymer for Printed Transistors. *Nature* **2009**, *457*, 679–686.
(13) Arias, A. C.; MacKenzie, J. D.; McCulloch, I.; Rivnay, J.; Salleo, A. Materials and Applications for Large Area Electronics: Solution-Based Approaches. *Chem. Rev.* **2010**, *110*, 3–24.
(14) Shtein, M.; Mapel, J.; Benziger, J. B.; Forrest, S. R. Effects of Film Morphology and Gate Dielectric Surface Preparation on the Electrical Characteristics of Organic-Vapor-Phase-Deposited Pentacene Thin-Film Transistors. *Appl. Phys. Lett.* **2002**, *81*, 268–270.
(15) Cornil, J.; Beljonne, D.; Calbert, J. P.; Brédas, J. L. Interchain Interactions in Organic Pi-Conjugated Materials: Impact on Electronic Structure, Optical Response, and Charge Transport. *Adv. Mater.* **2001**, *13*, 1053–1067.
(16) Liscio, A.; Orgiu, E.; Mativetsky, J. M.; Palermo, V.; Samorì, P. Bottom-up Fabricated Asymmetric Electrodes for Organic Electronics. *Adv. Mater.* **2010**, *22*, 5018–5023.
(17) Darmawan, P.; Minari, T.; Kumatani, A.; Li, Y.; Liu, C.; Tsukagoshi, K. Reduction of Charge Injection Barrier by 1-nm Contact Oxide Interlayer in Organic Field Effect Transistors. *Appl. Phys. Lett.* **2012**, *100*, 013303–013303–3.
(18) Stoliar, P.; Kshirsagar, R.; Massi, M.; Annibale, P.; Albonetti, C.; de Leeuw, D. M.; Biscarini, F. Charge Injection across Self-Assembly Monolayers in Organic Field-Effect Transistors: Odd–Even Effects. *J. Am. Chem. Soc.* **2007**, *129*, 6477–6484.
(19) Crivillers, N.; Orgiu, E.; Reinders, F.; Mayor, M.; Samorì, P. Optical Modulation of the Charge Injection in an Organic Field-Effect Transistor Based on Photochromic Self-Assembled-Monolayer-Functionalized Electrodes. *Adv. Mater.* **2011**, *23*, 1447–1452.
(20) Smits, E. C. P.; Mathijssen, S. G. J.; van Hal, P. A.; Setayesh, S.; Geuns, T. C. T.; Mutsaers, K. A. H. A.; Cantatore, E.; Wondergem, H. J.; Werzer, O.; Resel, R.; Kemerink, M.; Kirchmeyer, S.; Muzafarov, A. M.; Ponomarenko, S. A.; de Boer, B.; Blom, P. W. M.; de Leeuw, D. M. Bottom-up Organic Integrated Circuits. *Nature* **2008**, *455*, 956–959.
(21) Orgiu, E.; Crivillers, N.; Rotzler, J.; Mayor, M.; Samorì, P. Tuning the Charge Injection of P3HT-Based Organic Thin-Film Transistors through Electrode Functionalization with Oligophenylene SAMs. *J. Mater. Chem.* **2010**, *20*, 10798–10800.
(22) Hutchins, D. O.; Weidner, T.; Baio, J.; Polishak, B.; Acton, O.; Cernetic, N.; Ma, H.; Jen, A. K. Y. Effects of Self-Assembled Monolayer Structural Order, Surface Homogeneity and Surface Energy on Pentacene Morphology and Thin Film Transistor Device Performance. *J. Mater. Chem. C* **2013**, *1*, 101–113.
(23) Halik, M.; Klauk, H.; Zschieschang, U.; Schmid, G.; Ponomarenko, S.; Kirchmeyer, S.; Weber, W. Relationship between Molecular Structure and Electrical Performance of Oligothiophene Organic Thin Film Transistors. *Adv. Mater.* **2003**, *15*, 917–922.
(24) Payne, M. M.; Parkin, S. R.; Anthony, J. E.; Kuo, C. C.; Jackson, T. N. Organic Field-Effect Transistors from Solution-Deposited Functionalized Acenes with Mobilities as High as 1 $cm^2/V{\cdot}s$. *J. Am. Chem. Soc.* **2005**, *127*, 4986–4987.
(25) Sergeyev, S.; Pisula, W.; Geerts, Y. H. Discotic Liquid Crystals: A New Generation of Organic Semiconductors. *Chem. Soc. Rev.* **2007**, *36*, 1902–1929.
(26) Leufgen, M.; Rost, O.; Gould, C.; Schmidt, G.; Geurts, J.; Molenkamp, L. W.; Oxtoby, N. S.; Mas-Torrent, M.; Crivillers, N.; Veciana, J.; Rovira, C. High-Mobility Tetrathiafulvalene Organic Field-Effect Transistors from Solution Processing. *Org. Electron.* **2008**, *9*, 1101–1106.
(27) Mas-Torrent, M.; Masirek, S.; Hadley, P.; Crivillers, N.; Oxtoby, N. S.; Reuter, P.; Veciana, J.; Rovira, C.; Tracz, A. Organic Field-Effect Transistors (OFETs) of Highly Oriented Films of Dithiophene–Tetrathiafulvalene Prepared by Zone Casting. *Org. Electron.* **2008**, *9*, 143–148.
(28) Gao, P.; Beckmann, D.; Tsao, H. N.; Feng, X.; Enkelmann, V.; Baumgarten, M.; Pisula, W.; Müllen, K. Dithieno[2,3-*d*;2′,3′-*d*′]benzo-[1,2-*b*;4,5-*b*′]dithiophene (DTBTD) as Semiconductor for High-Performance, Solution-Processed Organic Field-Effect Transistors. *Adv. Mater.* **2009**, *21*, 213–216.
(29) Cavallini, M.; D'Angelo, P.; Criado, V. V.; Gentili, D.; Shehu, A.; Leonardi, F.; Milita, S.; Liscio, F.; Biscarini, F. Ambipolar Multi-Stripe Organic Field-Effect Transistors. *Adv. Mater.* **2011**, *23*, 5091–5097.
(30) Minemawari, H.; Yamada, T.; Matsui, H.; Tsutsumi, J. y.; Haas, S.; Chiba, R.; Kumai, R.; Hasegawa, T. Inkjet Printing of Single-Crystal Films. *Nature* **2011**, *475*, 364–367.
(31) Kobayashi, H.; Kobayashi, N.; Hosoi, S.; Koshitani, N.; Murakami, D.; Shirasawa, R.; Kudo, Y.; Hobara, D.; Tokita, Y.; Itabashi, M. Hopping and Band Mobilities of Pentacene, Rubrene, and 2,7-Dioctyl[1]benzothieno[3,2-B][1]benzothiophene (C8-BTBT) from First Principle Calculations. *J. Chem. Phys.* **2013**, *139*, 014707.
(32) Yuan, Y. B.; Giri, G.; Ayzner, A. L.; Zoombelt, A. P.; Mannsfeld, S. C. B.; Chen, J. H.; Nordlund, D.; Toney, M. F.; Huang, J. S.; Bao, Z. N. Ultra-High Mobility Transparent Organic Thin Film Transistors Grown by an Off-Centre Spin-Coating Method. *Nat. Commun.* **2014**, *5*, 3005.
(33) Horowitz, G.; Peng, X. Z.; Fichou, D.; Garnier, F. Organic Thin-Film Transistors Using Pi-Conjugated Oligomers—Influence of the Chain-Length. *J. Mol. Electron.* **1991**, *7*, 85–89.
(34) Garnier, F.; Horowitz, G.; Peng, X. Z.; Fichou, D. Structural Basis for High Carrier Mobility in Conjugated Oligomers. *Synth. Met.* **1991**, *45*, 163–171.
(35) Dodabalapur, A.; Torsi, L.; Katz, H. E. Organic Transistors—2-Dimensional Transport and Improved Electrical Characteristics. *Science* **1995**, *268*, 270–271.
(36) Katz, H. E.; Torsi, L.; Dodabalapur, A. Synthesis, Material Properties, and Transistor Performance of Highly Pure Thiophene Oligomers. *Chem. Mater.* **1995**, *7*, 2235–2237.
(37) Horowitz, G.; Fichou, D.; Peng, X. Z.; Xu, Z. G.; Garnier, F. A Field-Effect Transistor Based on Conjugated alpha-Sexithienyl. *Solid State Commun.* **1989**, *72*, 381–384.
(38) Biscarini, F.; Zamboni, R.; Samorì, P.; Ostoja, P.; Taliani, C. Growth of Conjugated Oligomer Thin-Films Studied by Atomic-Force Microscopy. *Phys. Rev. B* **1995**, *52*, 14868–14877.
(39) Leclère, P.; Surin, M.; Viville, P.; Lazzaroni, R.; Kilbinger, A. F. M.; Henze, O.; Feast, W. J.; Cavallini, M.; Biscarini, F.; Schenning, A.; Meijer, E. W. About Oligothiophene Self-Assembly: From Aggregation in Solution to Solid-State Nanostructures. *Chem. Mater.* **2004**, *16*, 4452–4466.
(40) Barbarella, G.; Melucci, M.; Sotgiu, G. The Versatile Thiophene: An Overview of Recent Research on Thiophene-Based Materials. *Adv. Mater.* **2005**, *17*, 1581–1593.
(41) Dinelli, F.; Capelli, R.; Loi, M. A.; Murgia, M.; Muccini, M.; Facchetti, A.; Marks, T. J. High-Mobility Ambipolar Transport in Organic Light-Emitting Transistors. *Adv. Mater.* **2006**, *18*, 1416–1420.
(42) Duhm, S.; Xin, Q.; Koch, N.; Ueno, N.; Kera, S. Impact of Alkyl Side Chains at Self-Assembly, Electronic Structure and Charge Arrangement in Sexithiophene Thin Films. *Org. Electron.* **2011**, *12*, 903–910.
(43) Ashizawa, M.; Niimura, T.; Yu, Y.; Tsuboi, K.; Matsumoto, H.; Yamada, R.; Kawauchi, S.; Tanioka, A.; Mori, T. Improved Stability of Organic Field-Effect Transistor Performance in Oligothiophenes Including β-Isomers. *Tetrahedron* **2012**, *68*, 2790–2798.
(44) Anokhin, D. V.; Defaux, M.; Mourran, A.; Moeller, M.; Luponosov, Y. N.; Borshchev, O. V.; Bakirov, A. V.; Shcherbina, M. A.; Chvalun, S. N.; Meyer-Friedrichsen, T.; Elschner, A.; Kirchmeyer, S.; Ponomarenko, S. A.; Ivanov, D. A. Effect of Molecular Structure of

α,α'-Dialkylquaterthiophenes and Their Organosilicon Multipods on Ordering, Phase Behavior, and Charge Carrier Mobility. *J. Phys. Chem. C* **2012**, *116*, 22727−22736.
(45) Katz, H. E.; Lovinger, A. J.; Laquindanum, J. G. a,ω-Dihexylquaterthiophene: A Second Thin Film Single-Crystal Organic Semiconductor. *Chem. Mater.* **1998**, *10*, 457−459.
(46) Generali, G.; Dinelli, F.; Capelli, R.; Toffanin, S.; di Maria, F.; Gazzano, M.; Barbarella, G.; Muccini, M. Correlation among Morphology, Crystallinity, and Charge Mobility in OFETS Made of Quaterthiophene Alkyl Derivatives on a Transparent Substrate Platform. *J. Phys. Chem. C* **2011**, *115*, 23164−23169.
(47) Song, D. H.; Choi, M. H.; Kim, J. Y.; Jang, J.; Kirchmeyer, S. Process Optimization of Organic Thin-Film Transistor by Ink-Jet Printing of DH4T on Plastic. *Appl. Phys. Lett.* **2007**, *90*, 053504.
(48) Garnier, F.; Hajlaoui, R.; El Kassmi, A.; Horowitz, G.; Laigre, L.; Porzio, W.; Armanini, M.; Provasoli, F. Dihexylquaterthiophene, a Two-Dimensional Liquid Crystal-like Organic Semiconductor with High Transport Properties. *Chem. Mater.* **1998**, *10*, 3334−3339.
(49) Moret, M.; Campione, M.; Borghesi, A.; Miozzo, L.; Sassella, A.; Trabattoni, S.; Lotz, B.; Thierry, A. Structural Characterisation of Single Crystals and Thin Films of α,ω-Dihexylquaterthiophene. *J. Mater. Chem.* **2005**, *15*, 2444−2449.
(50) Palermo, V.; Samorì, P. Molecular Self-Assembly across Multiple Length Scales. *Angew. Chem., Int. Ed.* **2007**, *46*, 4428−4432.
(51) Granstrom, E. L.; Frisbie, C. D. Field Effect Conductance Measurements on Thin Crystals of Sexithiophene. *J. Phys. Chem. B* **1999**, *103*, 8842−8849.
(52) Someya, T.; Katz, H. E.; Gelperin, A.; Lovinger, A. J.; Dodabalapur, A. Vapor Sensing with alpha,omega-Dihexylquarterthiophene Field-Effect Transistors: The Role of Grain Boundaries. *Appl. Phys. Lett.* **2002**, *81*, 3079−3081.
(53) Dabirian, R.; Palermo, V.; Liscio, A.; Schwartz, E.; Otten, M. B. J.; Finlayson, C. E.; Treossi, E.; Friend, R. H.; Calestani, G.; Müllen, K.; Nolte, R. J. M.; Rowan, A. E.; Samorì, P. The Relationship between Nanoscale Architecture and Charge Transport in Conjugated Nanocrystals Bridged by Multichromophoric Polymers. *J. Am. Chem. Soc.* **2009**, *131*, 7055−7063.
(54) De Luca, G.; Pisula, W.; Credgington, D.; Treossi, E.; Fenwick, O.; Lazzerini, G. M.; Dabirian, R.; Orgiu, E.; Liscio, A.; Palermo, V.; Müllen, K.; Cacialli, F.; Samorì, P. Non-Conventional Processing and Post-Processing Methods for the Nanostructuring of Conjugated Materials for Organic Electronics. *Adv. Funct. Mater.* **2011**, *21*, 1279−1295.
(55) Tanase, C.; Meijer, E. J.; Blom, P. W. M.; de Leeuw, D. M. Local Charge Carrier Mobility in Disordered Organic Field-Effect Transistors. *Org. Electron.* **2003**, *4*, 33−37.
(56) Dinelli, F.; Murgia, M.; Levy, P.; Cavallini, M.; Biscarini, F.; de Leeuw, D. M. Spatially Correlated Charge Transport in Organic Thin Film Transistors. *Phys. Rev. Lett.* **2004**, *92*, 116802.
(57) Chua, L. L.; Zaumseil, J.; Chang, J. F.; Ou, E. C. W.; Ho, P. K. H.; Sirringhaus, H.; Friend, R. H. General Observation of n-Type Field-Effect Behaviour in Organic Semiconductors. *Nature* **2005**, *434*, 194−199.